

# Optimal Source-Modulation Frequencies for Small-Geometry Frequency-Domain Optical Tomography

Hyun Keol Kim<sup>1</sup>, Uwe J. Netz<sup>3</sup>, J. Beuthan<sup>3</sup>, and Andreas H. Hielscher<sup>1,2</sup>

<sup>1</sup>Department of biomedical engineering, Columbia University, 351 Engineering Terrace., 500 West 120th St., New York, NY 10027

<sup>2</sup>Department of Radiology, Columbia University, 660 West 168th St., New York, New York 10327

<sup>3</sup>Institut für Medizinische Physik und Lasermedizin, Charité - Universitätsmedizin Berlin, Fabbeckstraße 60-62, 14195 Berlin, Germany  
e-mail address: ahh2004@columbia.edu

**Abstract:** In frequency-domain optical tomography, the reconstruction performance is affected by the choice of source-modulation frequency. To find optimal frequencies, we investigate here the frequency dependence of optical tomographic reconstruction results using the frequency-domain equation of radiative transfer. We present numerical and phantom studies with a focus on small tissue geometries. Best results were achieved in the 600-800MHz frequency range.

©2007 Optical Society of America

OCIS codes: (110.6955) Tomographic imaging; (170.4090) Modulation techniques

## 1. Introduction

Frequency domain optical tomography (FDOT) is an emerging imaging modality that has been applied to a wide variety of biomedical fields [1,2]. However, employing FDOT for imaging of small tissue volumes, such as small-animal or finger-joint imaging, possess a variety of challenges that have not yet been overcome. First of all most frequency-domain reconstruction codes are based on the diffusion approximation to the equation of radiative transfer [3]. This approximation, however, becomes questionable when applied to small tissue-geometries and is further compromised if highly absorbing objects or fluid-filled regions, which contain, for example, cerebrospinal or synovial fluids, are considered [4]. Transport-theory based codes that avoid the diffusion approximation can alleviate these problems, and first algorithms of this kind were recently developed [5-7].

But even with these codes in place, another challenge is to find optimal source-modulation frequencies at which to perform optical tomographic imaging. In small tissue geometries, the frequency-shift at small source-modulation frequencies is typically very small and difficult to measure. Increasing the modulation frequency leads to larger phase shifts, but at the same time the amplitude signal becomes smaller and smaller. Gu et al. [8] have studied these trade offs employing a transport-theory-based frequency-domain forward model. In numerical studies they have shown that for typical geometries encountered in small animal imaging, highest signal-to-noise-ratios (SNRs) can be achieved in the 400-600MHz frequency range. What has not yet been studied is how these different SNR values in the forward data affect the actual optical tomographic reconstructions. In the study at hand we employ an optical tomography code that is based on the frequency-domain equation of radiative transfer (ERT), to find source modulation frequencies that result in best image quality when small imaging domains are considered. We show results of numerical studies and experiments on tissue phantoms with well characterized optical properties.

## 2. Forward and inverse models

The frequency domain forward model for light propagation in tissue can be accurately modeled by the radiative transfer equation as [5-7]

$$[\Omega \cdot \nabla + \mu_a + \mu_s + i\frac{\omega}{c}]I(\vec{r}, \Omega, \omega) = \frac{\mu_s}{4\pi} \int_{4\pi} I(\vec{r}, \Omega^+, \omega) \Phi(\Omega^+, \Omega) d\Omega^+ \quad (1)$$

where  $I$  is radiation intensity in unit  $[W/cm^2/sr]$ , and  $\mu_a$  and  $\mu_s$  are the absorption and scattering coefficient in units of  $[cm^{-1}]$ , and  $\Phi$  is the phase function describing scattering from direction  $\Omega^+$  into direction  $\Omega$ . We use here the Henyey-Greenstein phase function that is commonly used in tissue optics. The partially-reflected boundary condition is implemented to consider the refractive index mismatch problem between the medium and the air as [9]. Also the node-centered finite volume method combined with the discrete ordinate method is applied to discretizing the forward model given by (1) into the spatial and angular domains [9]. The resulting sparse linear equation is iteratively solved for intensity into a discrete ordinate direction by using the restarted version of the GMRES solver [10].

In the reconstruction model involving with the complex-valued data, the objective function is defined as:

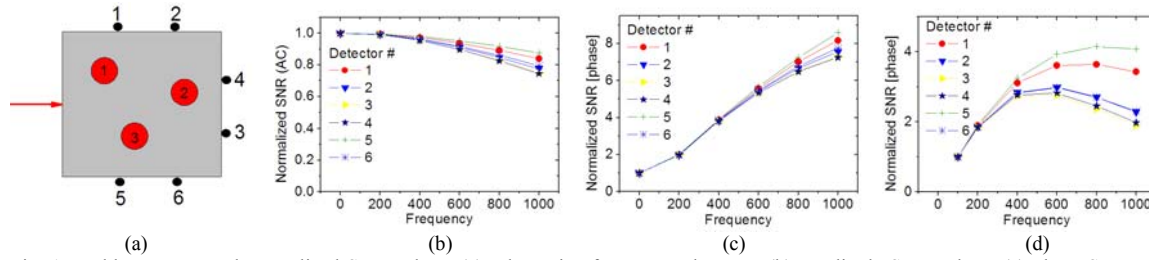


Fig. 1. Problem set up and normalized SNR values; (a) schematic of a square phantom; (b) amplitude SNR values; (c) phase SNR values. (d) same as (c), however,  $\mu_a$  of background was decreased to 0.1  $[\text{cm}^{-1}]$ . Note that each value is normalized to the value at 100Hz.

$$\phi[\mu_a, \mu_s] = \frac{1}{2} \sum_{s=1}^{N_s} \sum_{d=1}^{N_d} \frac{(M_{s,d} - P_{s,d}) \cdot (M_{s,d}^* - P_{s,d}^*)}{\sigma_{s,d} \cdot \sigma_{s,d}^*} \quad (2)$$

where  $N_s$  and  $N_d$  are numbers of the sources and the detectors respectively,  $\sigma$  is complex-valued standard deviations for each source-detector pair, and  $P_{s,d}$  ( $P_{s,d}^*$ ) and  $M_{s,d}$  ( $M_{s,d}^*$ ) are complex-valued predictions (complex conjugate) and measurements (complex conjugate), respectively. Note that the measured and predicted data given by (2) is the normalized. Also calculation of the gradient of the objective function with respect to the optical property, which is another central part of the optimization procedure, is performed with an adjoint formulation [5-6]. Finally the unknown optical properties are iteratively updated by using the limited-memory version of the BFGS optimization method [11].

To study the frequency dependency of the reconstruction results we consider the influence on the reconstruction quality. As a noise model, we use models introduced by Toronov et al and modified by Gu et al, given as [12]:

$$\text{SNR}_{AC} = \frac{\langle AC \rangle}{\sigma_{AC}} \propto \frac{\langle AC \rangle}{\sqrt{DC}}; \quad \text{SNR}_{\Phi} = \frac{\langle \Phi \rangle}{\sigma_{\Phi}} \propto \langle \Phi \rangle \text{SNR}_{AC} \quad (3)$$

According to the noise model given by (3), the standard deviations in the amplitude and in the phase are proportional to  $\sqrt{DC}$  and  $\sqrt{DC}/AC$ , respectively, i.e., the phase noise increases with the frequency. This model is used to assess the signal-to-noise ratio (SNR) for a geometry specific to our study that will be shown in later part of this paper.

### 3. Reconstructions and discussions

In this section we present the reconstruction results obtained with the normalized data. In the numerical as well as experimental studies we consider a 3cm-by-3cm square phantom with three inclusions shown in Fig. 1a. The first two inclusions are highly scattering while the other object is highly absorbing. The optical properties of the background medium are  $\mu_a = 0.62 \text{ cm}^{-1}$  and  $\mu'_s = 7.62 \text{ cm}^{-1}$ , while the two highly scattering inclusions are given  $\mu_a = 0.1 \text{ cm}^{-1}$  and  $\mu'_s = 25.7 \text{ cm}^{-1}$  and the purely absorbing object is given  $\mu_a = 1.2 [1/\text{cm}]$  and  $\mu'_s = 7.62 [1/\text{cm}]$ . First we look at the frequency dependence of the SNR at various detector positions. The results are shown in Fig. 1b-1c. Interestingly the SNR increases with a frequency in all positions, which looks somewhat different from the typical SNR curve that tends to show a maximum value at a particular frequency [8,12]. However, we found that the position of this maximum moves to higher frequencies as  $\mu_a$  is increased and  $\mu'_s$  is decreased. For example, Fig. 1d shows the same curves for a medium with a background  $\mu_a = 0.1 \text{ cm}^{-1}$ . Here the maximum value occurs  $\sim 600 \text{ MHz}$ .

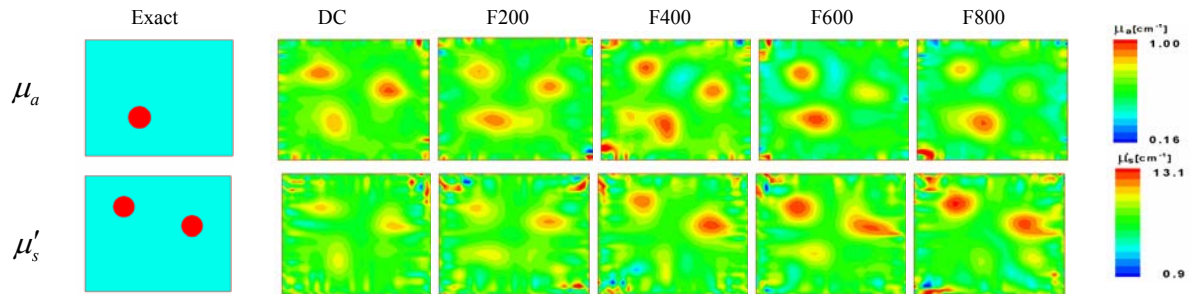


Fig. 2 Reconstruction results from using different frequencies; 0, 200, 400, 600 and 800MHz.

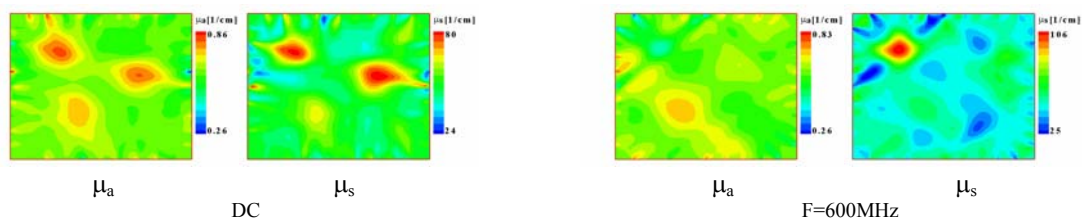


Fig. 3. Reconstruction results from the real phantom data measured at DC and frequency 600MHz.

Next we performed reconstructions at various frequencies to determine which yields the best separation between the objects by reducing the cross-talk problem. The noise-added synthetic data is generated by applying the noise model given in Eq. (3). Furthermore we normalize both amplitude and phase independently for measurements on each side of the square phantom, since the experimental data was obtained in this way. The reconstruction procedure is started with an initial guess set identical to the optical properties of the background medium. As seen in Fig. 2 there is considerable cross-talk between scattering and absorbing objects in the DC case ( $\omega = 0$  MHz). Therefore, the two scattering inhomogeneities appear in the absorption maps and the absorbing object also appears in the scattering reconstruction. As  $\omega$  is increased the cross-talk is greatly reduced and the reconstruction separates the absorbing and scattering objects. However, at 1 GHz the SNR in the forward data becomes so poor that the code does not converge anymore and no useful image is obtained. In this particular case the images at 600MHz and 800MHz show the best results.

In addition to these numerical results, we also studied the retrieval of optical properties inside a real phantom with optical properties identical to those in our numerical studies. The measurement data was obtained at  $\omega = 600$ MHz, which yields a reasonable amplitude SNR using our instrument and provides for large enough phase shifts that can be measured with sufficient SNR. The reconstruction results are given in Fig. 3 for the DC and 600MHz data. As found in the numerical study, the DC data reveals strong crosstalk due to highly scattering objects. Using the 600MHz data the cross-talk is greatly diminished. However, in this particular case only one of the scattering objects is retrieved, which suggests that the noise in the current system is still too strong, or more views are necessary. Ongoing studies are addressing this issue in more details. It is also planned to extend this study to measurement and reconstruction of data obtained from small animals and finger joints.

This work was supported in part by the National Institute of Arthritis and Musculoskeletal and Skin Diseases (NIAMS-2R01-AR046255) and the National Institute for Biomedical Imaging and Bioengineering (NIBIB-R01-001900).

#### Reference:

- [1] M.A. O'Leary, D.A. Boas, B. Chance and A.G. Yodh, "Experimental images of heterogeneous turbid media by frequency-domain diffusion photon tomography", *Opt. Lett.* 20, 426-428(1995).
- [2] S. Nioka, Y. Yung, M. Shnall S. Zhao, S. Orel, C. Xie, B. Chance and L. Solin, "Optical imaging of breast tumor by means of continuous waves", *Adv. Exp. Med. Biol.* 411, 227-232(1997).
- [3] M.S. Patterson, "Optical image reconstruction using frequency domain data: Simulations and experiments", *J. Opt. Soc. Am. A* 13, 253-266(1996).
- [4] A. H. Hielscher, A. E. Alcouffe, and R. L. Barbour, "Comparison of finite-difference transport and diffusion calculations for photon migration in homogeneous and heterogeneous tissues," *Phys. Med. Biol.* 43, 1285-1302 (1998).
- [5] K. Ren and A. Hielscher, "Frequency domain optical tomography based on the equation of radiative transfer," *SIAM J. Sci. Comp.*, 28, 1463-89(2006).
- [6] H. K. Kim and A. Charette, "A sensitivity function-based conjugate gradient method for optical tomography with the frequency-domain equation of radiative transfer," *J. Quant. Spec. Rad. Trans.* 104, 24-39(2007).
- [7] G. Abdoulaev, K. Ren and A. Hielscher, "Optical tomography as a PDE-constrained optimization problem", *Inverse Problems* 21, 1507-1530(2005).
- [8] X. Gu, K. Ren, A.H. Hielscher, "Frequency-domain sensitivity analysis for small imaging domains using the equation of radiative transfer," *Applied Optics* 46 (10), pp. 1624-1632 (2007).
- [9] M. F. Modest, *Radiative Heat Transfer*, McGraw-Hill, New York, 1993.
- [10] Y. Saad, "GMRES: A generalized minimum residual algorithm for solving nonsymmetric linear systems," *SIAM Journal of Scientific and Statistical Computing* 7, 856-869(1986).
- [11] J. Nocedal and S. J. Wright, *Numerical optimization*, Springer-Verlag, New York, 1999.
- [12] V. Toronov, E. D'Amico, D. Hueber, E. Gratton, B. Barbieri, and A. Webb, "Optimization of the signal-to-noise ratio of frequency domain instrument for near-infrared spectro-imaging of the human brain," *Opt. Express* 11, 2117-2729 (2003).